JACS
JOURNAL OF THE AMERICAN CHEMICAL SOCIETY
Article
pubs.acs.org/JACS

Tunneling Electrical Connection to the Interior of Metal–Organic Frameworks

Shuangbing Han,[†,‡,⊥] Scott C. Warren,[§,⊥] Seok Min Yoon,[∥,⊥] Christos D. Malliakas,[‡] Xianliang Hou,[†,‡] Yanhu Wei,[†,‡] Mercouri G. Kanatzidis,[‡] and Bartosz A. Grzybowski*[,∥]

[†]Department of Chemical and Biological Engineering and [‡]Department of Chemistry, Northwestern University, Evanston, Illinois 60208, United States

[§]Department of Chemistry and Department of Applied Physical Sciences, University of North Carolina at Chapel Hill, Chapel Hill, North Carolina 27599, United States

[∥]IBS Center for Soft and Living Matter and the Department of Chemistry, Ulsan National Institute of Science and Technology (UNIST), Ulsan, South Korea

Supporting Information

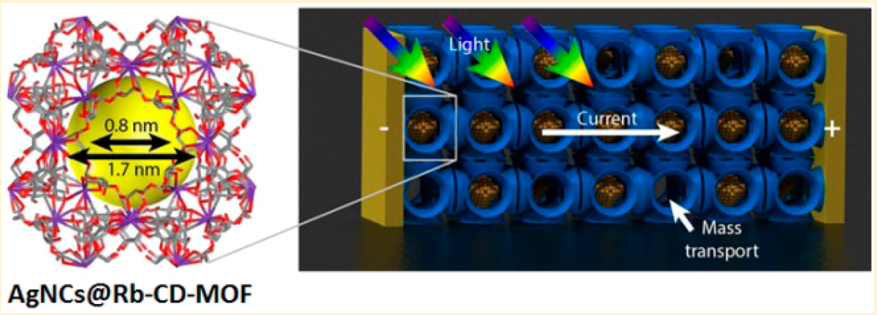

ABSTRACT: Metal–organic frameworks (MOFs) are typically poor electrical conductors, which limits their uses in sensors, fuel cells, batteries, and other applications that require electrically conductive, high surface area materials. Although metal nanoclusters (NCs) are often added to MOFs, the electrical properties of these hybrid materials have not yet been explored. Here, we show that adding NCs to a MOF not only imparts moderate electrical conductivity to an otherwise insulating material but also renders it photoconductive, with conductivity increasing by up to 4 orders of magnitude upon light irradiation. Because charge transport occurs via tunneling between spatially separated NCs that occupy a small percent of the MOF's volume, the pores remain largely open and accessible. While these phenomena are more pronounced in single-MOF crystals (here, Rb-CD-MOFs), they are also observed in films of smaller MOF crystallites (MIL-53). Additionally, we show that in the photoconductive MOFs, the effective diffusion coefficients of electrons can match the typical values of small molecules diffusing through MOFs; this property can open new vistas for the development of MOF electrodes and, in a wider context, of electroactive and light-harvesting MOFs.

INTRODUCTION

In addition to their applications in gas storage, molecular separations, and catalysis,[1−3] there is an increasing interest in metal–organic frameworks (MOFs) that might operate as porous electrodes or membranes in batteries,[4,5] fuel cells,[6] solar energy conversion,[7] supercapacitors,[8,9] and sensors.[10] In order to apply the full range of MOF architectures to construct novel materials for these devices, a simple and generalizable strategy is needed to produce electrically conductive MOFs.[11−14] So far, two strategies have emerged, albeit with significant limitations. In the first strategy, the MOF is constructed from redox-active metal centers,[13,15] molecular donor–acceptor pairs,[10,11] or π-conjugated molecules.[16−18] Although this approach occasionally yields MOFs with modest electrical conductivity and open porosity,[19] at present there are very few MOF building blocks with the requisite charge-transport properties.[17,20,21] As a result, one of the greatest strengths of MOFs—the great variety of their structures and properties—cannot be exploited with this approach. In the second strategy, the MOF's pores are backfilled with an electrically conductive material.[11,22−24] Although this strategy has been applied to many MOF architectures, in almost every case the MOF loses its porosity. Consequently, neither approach provides a simple route to simultaneously achieve within most MOFs efficient electrical and mass transport; this combination of transport properties is desirable for using MOFs as potential components of electrochemical devices including batteries, fuel cells, or MOF based memories.[25] In such devices, inefficiencies accumulate[26] in the form of, among others, voltage losses due to slow mass

Received: March 29, 2015
Published: May 28, 2015

DOI: 10.1021/jacs.5b03263
J. Am. Chem. Soc. 2015, 137, 8169−8175

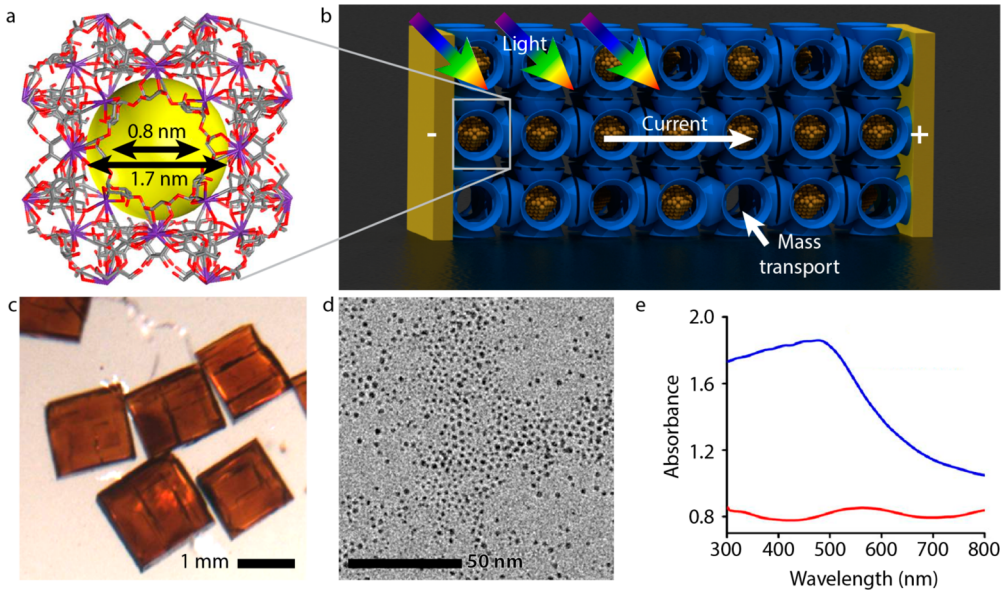

Figure 1. (a) A unit cell of a Rb-CD-MOF crystal synthesized from γ-CD and RbOH. The yellow sphere indicates a ∼1.7 nm cavity; the channels connecting the cavities are ∼0.8 nm wide. (b) Schematic representation of Ag nanoclusters deposited by immersing Rb-CD-MOF crystals in CH_3CN solution of $AgNO_3$. Not all cavities contain nanoclusters. (c) Optical images of AgNC@Rb-CD-MOF crystals (d) TEM image of AgNCs liberated upon dissolving AgNC@ Rb-CD-MOF in water. (e) Red curve is the UV−vis adsorption spectrum of a blank Rb-CD-MOF crystal. Blue curve is the spectrum of the same crystal "doped" with AgNCs (using 10 mM $AgNO_3$); notice the broad adsorption peak ranging from 300 to 550 nm.

transport, ΔE_{mass}, and losses due to resistive electrical transmission, ΔE_{ohmic}. Because of angstrom-to-nanometer-sized pores, mass transfer losses are an intrinsic limitation of MOFs and may always be a large contributor to device inefficiency. On the other hand, one can strive to minimize electrical losses such that $\Delta E_{ohmic} < \Delta E_{mass}$. In the Supporting Information (SI), Section 2 we show that this design heuristic translates into the requirement that diffusion coefficients of electrons be greater than diffusion coefficients of the ions/molecules diffusing through a MOF, $D_e > D_{mol}$. With diffusion coefficients in MOFs ranging from 10^{-14} to 10^{-7} cm^2/s, it can be estimated that this condition would be met if electrical conductivities of MOFs were above 10^{-11} to 10^{-5} S/cm (depending on the diffusing molecule, see SI, Section 2 and Table S1 therein).

In the present work, we describe a generalizable strategy to fabricate MOFs that achieve these conductivity targets with the help of light-assisted electron transport. Our approach relies on the formation of metal nanoclusters (NCs) distributed sparsely over the pores of MOFs. Unlike in previous strategies that relied on continuous electrical pathways, electrical transport in our NC-MOFs occurs via tunneling between the NCs; remarkably, the conductance of these hybrid materials increases by up to 4 orders of magnitude upon light irradiation. At the same time, a low volume fraction of the NCs within the MOFs ensures that the majority of the pores remain open and accessible, thus enabling mass transfer to the MOFs interior. Our approach provides a technically straightforward and generalizable route to lightweight materials combining conductivity and photoconductivity as well as molecular-scale porosity.

RESULTS AND DISCUSSION

In most experiments (cf. SI, Section 1, for the summary of experimental methods), we used millimeter-sized rubidium γ-cyclodextrin MOF single crystals (Rb-CD-MOF) that had silver NCs deposited in their pores. By using large single crystals, we were able to examine the intrinsic charge-transport properties of these materials without the influence of grain boundaries. The Rb-CD-MOF crystals, which have ∼1.7 nm cavities connected by ∼0.8 nm channels (Figure 1a), were synthesized from RbOH and γ-cyclodextrin (γ-CD) according to our previously published procedure.[27,28] Silver nanoclusters, AgNCs, were deposited in the MOFs (Figure 1b) by immersing the freshly synthesized Rb-CD-MOF crystals in a CH_3CN solution of 2 mM, 5 mM, or, in most experiments, 10 mM $AgNO_3$ for 48 h. As described before, the hydroxide anions in Rb-CD-MOFs can work either alone or cooperatively with cyclodextrins to reduce Ag^+ to AgNCs.[28] When this happens, the Rb-CD-MOF crystals turn brown-orange (Figure 1c) but retain their crystalline nature (cf. PXRD spectra in the SI, Section 3). The UV−vis spectra of such loaded crystals feature a broad adsorption peak between 300 and 550 nm (Figure 1e), which is due to the discrete optical transitions exhibited by metal NCs.[29,30] Transmission electron microscopy (TEM) images in Figure 1d indicate that the sizes of NCs in the MOFs are ca. 2 nm (for high-resolution image and particle size distribution, see ref 28). However, because TEM imaging damages the MOF and causes nanoparticle coalescence, the real particle size is smaller than the size observed during imaging. This sizing is also corroborated by high-angle annular dark-field scanning transmission electron microscopy in which individual particles inside the MOF can be seen (although, again, the high electron beam intensity causes particle coalescence during imaging, see Figure S3). Inductively coupled plasma atomic emission spectroscopy (ICP-AES) and energy-dispersive X-ray spectroscopy (EDX) allowed the loading of AgNCs to be determined as 0.67 vol % for 2 mM $AgNO_3$, 1.03 vol % for 5 mM $AgNO_3$, and 1.4 vol % for 10 mM $AgNO_3$ (see SI, Section 3). Importantly, at all of these loadings, the MOFs retain their high porosity, > 600 m^2/g, as verified by the BET data in the SI, Section 4.

DOI: 10.1021/jacs.5b03263
J. Am. Chem. Soc. 2015, 137, 8169−8175

Conductivity measurements were performed by covering two opposite facets of a MOF crystal with a thin (~ hundreds of μm in thickness) layer of conductive, quick-drying silver paste and connecting to a Keithley 6517B electrometer used to record the current–voltage, $I-V$, characteristics. In most measurements, we chose relatively thin AgNC@Rb-CD-MOF crystals (~100 μm) to ensure that light could penetrate the entire crystal. All crystals were degassed at <0.1 mTorr for at least 48 h to remove trace solvents from the MOF matrix. To eliminate effects of moisture and oxygen (which alter conductivity and can damage the MOF), the experiments were performed in a high-vacuum MMR chamber at <0.1 mTorr (for experiments under Ar flow, see SI, in Sections 5 and 6).

Both blank Rb-CD-MOFs and AgNC@Rb-CD-MOFs exhibited ohmic $I-V$ characteristics in the dark and under light irradiation (Figure 2 b). For the blank MOFs, dark

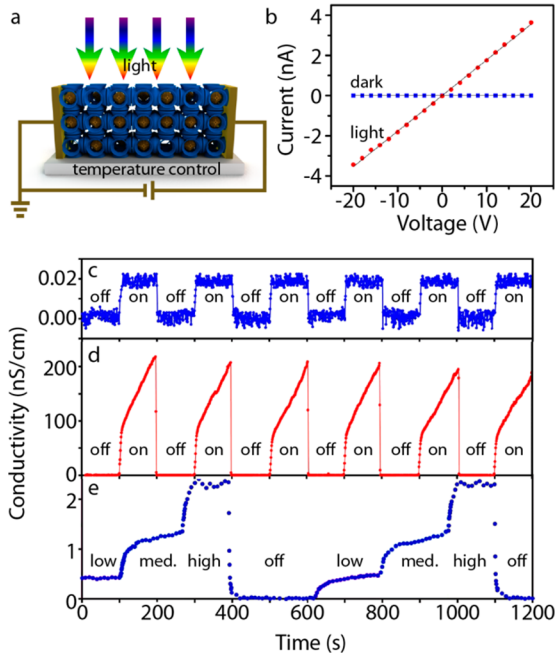

Figure 2. (a) Illustrates the experimental arrangement for measuring photoconductance of MOF crystals. (b) Two examples of $I-V$ characteristics of AgNC@Rb-CD-MOF crystals under light irradiation (630 mW/cm^2) and in the dark. The conductivities are, respectively, 1.8×10^{-8} and $\sim 2 \times 10^{-11}$ S cm^{-1}. Changes in the conductivity of (c) a blank Rb-CD-MOF and (d) a AgNC@Rb-CD-MOF over several irradiation cycles (here, power intensity 1.48 W/cm^2, crystals under vacuum, < 0.1 mTorr). (e) An example of conductivity changes recorded when AgNC@Rb-CD-MOF is exposed to light of different power intensities (low = 314 mW/cm^2, 320 K; med = 386 mW/cm^2, 326 K; high = 430 mW/cm^2, 333 K) under vacuum; <0.1 mTorr). Note that temperature of the crystal increases with increasing light intensity; effects of heating and purely optical excitation are summarized in Figure 3. All AgNC@Rb-CD-MOFs used here were made by immersing Rb-CD-MOFs in 10 mM $AgNO_3$.

conductivity was very low, $\sim 10^{-12}$ S cm^{-1}, and increased to only $\sim 2 \times 10^{-11}$ S cm^{-1} upon the highest irradiation power we used, 1.48 W/cm^2 (Figure 2c). In sharp contrast, the NC-doped MOFs (from 10 mM $AgNO_3$) had dark conductivity of $\sim 2 \times 10^{-11}$ S cm^{-1} which upon 1.48 W/cm^2 irradiation increased by about 4 orders of magnitude, to 2.15×10^{-7} S cm^{-1}. In these experiments, however, the impinging light caused both optical excitation and temperature increase, both of which contribute to increased conductivity (cf. Figure 2e, see also SI, Section 5). This interdependence—sometimes overlooked in studying photoconductance phenomena[31−33]—calls for more detailed studies aimed to separate the effects of light proper from the effects of light-induced heating.

Accordingly, to differentiate between direct optical excitation and thermal excitation, we measured the conductivity of the same AgNC@Rb-CD-MOF samples under constant light intensity but at different temperatures and at a constant temperature but under different light intensities. The samples were placed on a heating stage in the MMR chamber. A K20 programmable temperature controller (±0.1K) was used to control the temperature of the heating stage, and a chromel–alumel (type K) thermocouple was used to monitor the temperature of the sample *in situ*. The samples were irradiated with a white light illuminator (Model: Fiber-lite MI-150) through the optical window of the MMR chamber (see Figure S6). All of these measurements were performed for light intensities <700 mW/cm^2 for which the MOFs were confirmed to be structurally stable and the dark-light cycles were repeatable (for higher intensities and nonrepeatable cycling, see SI, Section 7).

Illustrative examples of these studies are shown in Figure 3. Figure 3a shows that upon temperature increase at constant light intensity of 314 mW/cm^2, the AgNC@Rb-CD-MOFs retained their ohmic $I-V$ characteristics, but their conductivity increased, for the curves shown, from 6.8×10^{-10} S/cm at 330 K to 3.1×10^{-9} S/cm at 350 K. As illustrated in Figure 3c, this increase was approximately exponential (with the rate of 7.7% per °C) and characterized by an activation energy of 0.77 eV (Figure 3e). The ohmic characteristics were also observed for different light intensities but at constant temperature; for instance, in Figure 3b, the conductivity increased from 3.6×10^{-9} to 1.47×10^{-8} S/cm when light intensity increased from 314 to 595 mW/cm^2 at 352 K (Figure 3b). The conductivity vs light-intensity dependence is shown in Figure 3d. Anticipating our discussion of the charge-transport mechanism, we also note that for MOFs containing different amounts of NCs (from 2, 5, and 10 mM $AgNO_3$ solutions), their conductivity decreased exponentially with the inverse cube root of the AgNC volume fractions, $\nu^{-1/3}$, determined by ICP-AES and EDX (cf. above and SI, Section 3); the plot of this dependence is included in Figure S8.

Together, the above data are evidence that there are two distinct excitation mechanisms in our materials that lead to enhanced electrical conductivity: a direct optical excitation and an indirect thermal excitation. To get further mechanistic insights into the origin of these phenomena, we plotted the dependencies—in the dark and under irradiation—of the logarithm of conductivity as a function of inverse temperature. As shown in Figure 3e,f, these plots are linear indicating Arrhenius-type relationships for both conditions. The activation energy, E_a, in the dark extracted from the Arrhenius plot in Figure 3f is about 0.92 eV (deviations in different samples do not exceed ~4%), and the value of E_a under light irradiation extracted from the Arrhenius plot in Figure 3e is about 0.77 eV (and within ~3% across different samples).

The observed activation energies are larger than typical values characterizing tunneling through arrays of metal nanoparticles.[34−36] On the other hand, an activation energy of as much as 0.7 eV has been measured in a film of metal nanoclusters, which was consistent with a model of activated tunneling.[37] In such a model (Figure 4a), tunneling is preceded

DOI: 10.1021/jacs.5b03263
J. Am. Chem. Soc. 2015, 137, 8169−8175

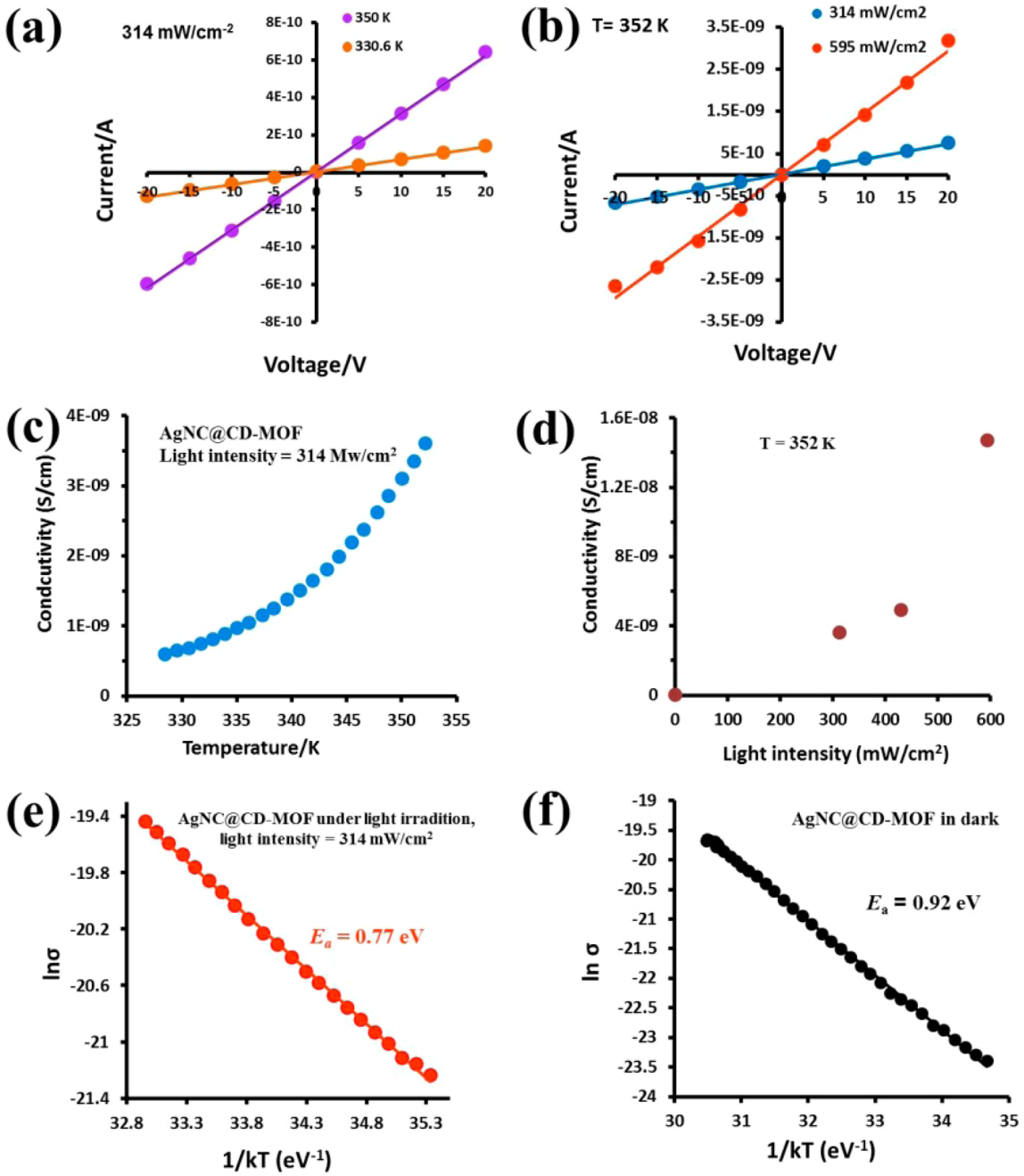

Figure 3. (a) Examples of the $I-V$ characteristics of AgNC@Rb-CD-MOF measured at different temperatures—here, 330.6 and 350 K—under light irradiation of the same intensity (314 mW/cm^2). (b) The $I-V$ dependencies for AgNC@Rb-CD-MOF under irradiation with light of different intensities (314 and 595 mW/cm^2) but at constant temperature (T = 352 K). (c) The temperature dependence of AgNC@Rb-CD-MOF conductivity at constant light intensity (314 mW/cm^2). (d) The light intensity dependence of AgNC@Rb-CD-MOF conductivity at constant temperature (352 K). (e) The natural logarithm of conductivity of AgNC@Rb-CD-MOF plotted as a function of inverse temperature at constant light intensity of 314 mW/cm^2. The linearity of this semilogarithmic plot indicates an Arrhenius relationship, and the slope gives the activation energy of 0.77 eV. (f) The Arrhenius relationship between dark conductivity of AgNC@Rb-CD-MOF and inverse temperature; the activation energy is 0.92 eV. All AgNC@Rb-CD-MOFs used here made by immersing Rb-CD-MOFs in 10 mM $AgNO_3$.

by the input of an activation energy because the energy of a system cannot change during tunneling and because the state that follows electron transfer is higher in energy than the state that precedes it. The activation energy, E_a, can be approximated by the energy needed to transform two neutral particles into a pair of oppositely charged particles; this energy is, in turn, a function of three parameters: (1) the radius, r, of the nanoparticles, (2) the distance that separates them, s, and (3) the dielectric constant, ε, of the medium:[35]

$$E_a = \frac{e^2}{8\pi\varepsilon_0\varepsilon}\frac{s}{r(r+s)} \quad (1)$$

where ε_0 is the permittivity of vacuum. Furthermore, we note that for a given metal loading, s depends on r. In order to determine the relationship between s and r, we developed a model in which the cavity sites of the Rb-CD-MOF (arranged on a bcc lattice and each having eight first nearest neighbors) are randomly occupied by the NCs (see SI, Section 9 for full

DOI: 10.1021/jacs.5b03263
J. Am. Chem. Soc. 2015, 137, 8169−8175

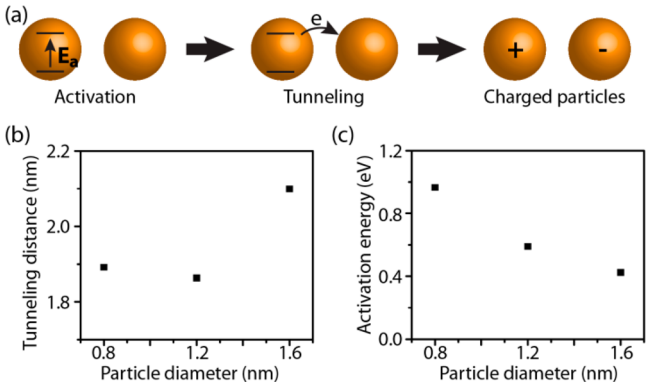

Figure 4. (a) Scheme of activation, tunneling, and generation of mobile charge carriers. (b) Modeled results showing the dependence of the average tunneling distance to a particle's first nearest neighbor as a function of particle diameter at 1.4 v/v% loading. (c) Calculated activation energy for tunneling between adjacent metal particles.

details of the model). The probability that a cavity site is occupied depends on the particle size and the experimentally measured metal loading. We considered three possible sizes of Ag particles: 0.8 nm, which is the same as the diameter of the apertures that connect MOF's cavities; 1.6 nm, which is just smaller than the inner diameter of the cavity; and 1.2 nm, an intermediate size. For the experimental 1.4 v/v% loading, 0.8 nm particles occupy 32% of the MOF cavity sites, allowing electrons to traverse the material exclusively by tunneling between the occupied nearest-neighbor sites. This conclusion can be understood from percolation theory, where a site percolation model (allowing for tunneling only to nearest-neighbor sites) predicts that at least 24.5% of sites must be occupied for electronic percolation to occur.[38] Particles with a diameter of 1.2 nm occupy ~10% of sites, and so electronic percolation cannot be achieved solely by tunneling to the first nearest-neighbor sites. In fact, our model shows that for such a loading, electronic percolation can occur only when tunneling to first, second, and third nearest neighbors takes place (see SI, Section 9). For 1.6 nm particles, tunneling to the first through sixth nearest neighbors is needed for electronic percolation. For each of these different percolation networks, we also calculated the average tunneling distance to the nearest-neighboring particle, since activation via charge transfer to the closest particle requires the smallest activation energy according to eq 1 (Figure 4b). Regardless of particle size, the average surface-to-surface distance between nearest-neighbor particles is about 2 nm (Figure 4b), which reflects two countervailing trends: (i) as the particle diameter increases, the site occupancy necessarily decreases, thereby increasing the average center-to-center distance to the first nearest-neighboring particle; and (ii) as the particle diameter increases, the average surface-to-surface distance between two particles (for example, nearest-neighbor sites) decreases. Although the likelihood of finding two particles on, e.g., nearest-neighbor sites, is lower in the system with larger particles (refer to the first trend), in those instances when there are particles with the same center-to-center distance, the average surface-to-surface distance is smaller. Most importantly, with an estimated dielectric constant of 1.54 for CD-MOF,[39−41]

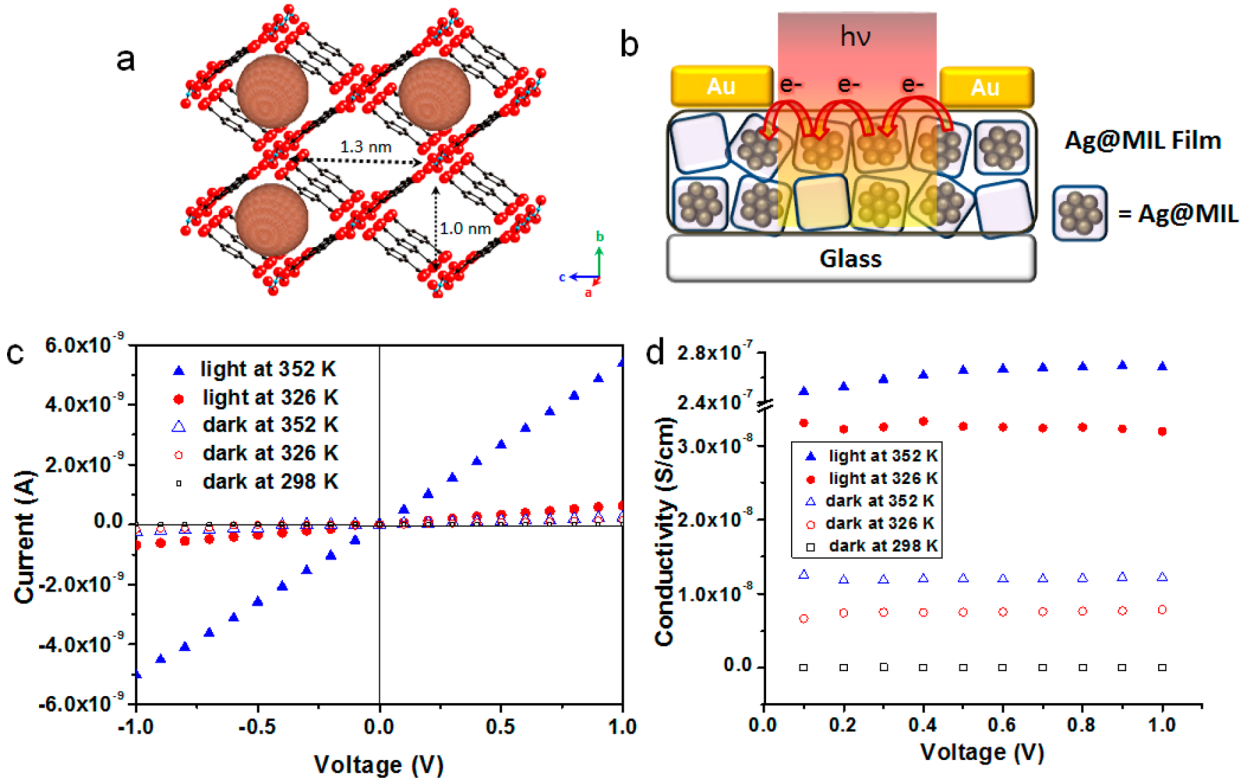

Figure 5. (a) A molecular cartoon illustrating the structure of a MIL-53 MOF with some sites occupied by AgNCs. (b) Scheme of experimental arrangement for measuring the photoconductance of the AgNC@MIL-53 film based (for additional schemes and images, see SI, Section 9) . (c) Representative *I*−*V* plots for dark current measured at 298 K (black open markers), 326 K (red open markers), and 352 K (blue open markers), and for photocurrent measured at 326 and 352 K (solid red and blue markers, respectively), in both cases under 595 mW/cm^2 white-light irradiation. The corresponding conductivities are plotted in (d). Notice a marked increase in the conductivity (to 2.67 × 10^{-7} S/cm) under irradiation at 352 K.

DOI: 10.1021/jacs.5b03263
J. Am. Chem. Soc. 2015, 137, 8169−8175

our model predicts that the observed activation energies 0.7−0.9 eV are consistent with the presence of ∼1 nm Ag particles. We note that this size is small enough to be occluded in MOF's cavities yet large enough to restrict NC movement through the MOF's 0.8 nm channels. Also, the predictions of the model are in line with the observed exponential decrease of conductivity with the inverse cube root of the AgNC volume fraction, $\nu^{-1/3}$ (cf. Figure S8). Based on our previous work[28] and the fact that MOF cavities and apertures limit nanoparticle growth, it is reasonable to assume that NC size is approximately independent of the metal volume fraction. Then, $\nu^{-1/3}$ is proportional to the average distance between nanoparticles and so the conductivity decreases exponentially with increasing distance between nanoparticles. This result is consistent with a model of electron tunneling, since the tunneling current decreases exponentially with increasing tunneling distance.[42]

The last question we wish to address is whether our approach can be generalized to other types of MOFs and/or films of smaller MOF crystallites (which are more popular than large single crystals). For these experiments, we chose commercially available MIL-53 MOF[43,44] (Basolite A100, Sigma-Aldrich) which we infiltrated with AgNCs following the procedure developed by Houk et al.[43] and summarized in the SI, Section 1. This procedure gave crystals with ca. 70% of the vacant cavity space occupied by AgNCs (Figure 5a) and with surface area of 37.3 m^2/g compared to 124.5 m^2/g for the native MIL-53 (see Figure S10 for BET isotherms). PXRD data in Figure S11 indicated that infiltration with the NCs did not cause any significant changes in the crystalline nature of the MOF. Importantly, the films of such NC-loaded MIL-53 crystals (Figures 5b and S12) exhibited increased conductivity both upon temperature increase and upon irradiation with light. However, these increases were more moderate than observed in single crystals, for example, at 326 K, irradiation of the film with 595 mW/cm^2 light increased the conductivity only 4.3 times, from 7.52×10^{-9} to 3.24×10^{-8} S/cm. The increase was more pronounced at higher temperature; at 352 K, the conductivity increased 22.3 times (from 1.19×10^{-8} S/cm to 2.67×10^{-7} S/cm at 352 K) upon 595 mW/cm^2 irradiation, likely because of a synergistic effect of light- and heat-assisted tunneling, as discussed earlier in the paper. The fact that conductivity increases in this system are more moderate than in the single crystals is not unexpected given that the grain boundaries between individual crystallites introduce an additional series resistance to the intrinsic charge transfer resistance of the Ag NC-loaded MOF.[45] Still, within each crystal, the mechanism of light assisted tunneling is operative, as detailed for the single-crystal Rb-CD-MOF studies.[46]

To summarize, although the ability to fabricate MOFs with virtually any chemical structure makes them compelling for many applications, there have only been a handful of MOFs that are inherently conductive. In this work, we showed that light-assisted electrical tunneling provides a charge-transport network that can deliver electrons to the interior of a MOF at rates comparable to the rate of mass transfer within a MOF pore. This represents the first general strategy for achieving electrical conductivity—and photoconductivity—and combining it with porosity regardless of the MOF architecture. We expect that this concept will enable the design of new materials such as composite electrocatalysts and photoelectrocatalysts in which the MOF catalyzes electrochemical reactions on the nanoparticle surface, such as the proton-coupled electron-transfer reactions that are essential to energy conversion.[47] Moreover, because tunneling depends sensitively on the dielectric constant,[35] these materials can act as detectors and photodetectors responding to subtle variations in the composition of the fluids or gases entering the MOF's pores.

■ ASSOCIATED CONTENT

Supporting Information

Experimental section and additional data. The Supporting Information is available free of charge on the ACS Publications website at DOI: 10.1021/jacs.5b03263.

■ AUTHOR INFORMATION

Corresponding Author

*grzybor72@unist.ac.kr

Author Contributions

⊥These authors contributed equally.

Notes

The authors declare no competing financial interest.

■ ACKNOWLEDGMENTS

This work was performed on the premises of Northwestern University under the support of the Nonequilibrium Energy Research Center which is an Energy Frontier Research Center funded by the U.S. Department of Energy, Office of Science, Office of Basic Energy Sciences under award number DE-SC0000989. S.M.Y. and B.A.G. gratefully acknowledge personal support from the Institute for Basic Science Korea, Project Code IBS-R020-D1. We thank Dr. Bartlomiej Kowalczyk for his help with TEM imaging and useful discussions in the early stages of this project.

■ REFERENCES

(1) Long, J. R.; Yaghi, O. M. *Chem. Soc. Rev.* **2009**, *38*, 1213−1214.
(2) Li, J.-R.; Kuppler, R. J.; Zhou, H.-C. *Chem. Soc. Rev.* **2009**, *38*, 1477−1504.
(3) Rowsell, J. L. C.; Yaghi, O. M. *Angew. Chem., Int. Ed.* **2005**, *44*, 4670−4679.
(4) Férey, G.; Milange, F.; Morcrette, M.; Serre, C.; Doublet, M. L.; Grenèche, J. M.; Tarascon, J. M. *Angew. Chem., Int. Ed.* **2007**, *46*, 3259−3263.
(5) Wiers, B. M.; Foo, M.-L.; Balsara, N. P.; Long, J. R. *J. Am. Chem. Soc.* **2011**, *133*, 14522−14525.
(6) Nohra, B.; Moll, H. E.; Albelo, L. M. R.; Mialan, P.; Marrot, J.; Draznieks, C. M.; O'Keeffe, M.; Biboum, R. N.; Lemaire, J.; Keita, B.; Nadjo, L.; Dolbecq, A. *J. Am. Chem. Soc.* **2011**, *133*, 13363−13374.
(7) Wang, C.; Xie, Z.; deKrafft, K. E.; Lin, W. *J. Am. Chem. Soc.* **2011**, *133*, 13445−13454.
(8) Lee, D. Y.; Yoon, S. J.; Shrestha, N. K.; Lee, S. H.; Ahn, H.; Han, S. H. *Microporous Mesoporous Mater.* **2012**, *153*, 163−165.
(9) Díaz, R.; Orcajo, M. G.; Botas, J. A.; Calleja, G.; Palma, J. *Mater. Lett.* **2012**, *68*, 126−128.
(10) Kreno, L. E.; Kreno, L. E.; Leong, K.; Farha, O.; Allendorf, M.; Van Duyne, R. P.; Hupp, J. T. *Chem. Rev.* **2011**, *112*, 1105−1125.
(11) Talin, A. A.; Centrone, A.; Ford, A. C.; Foster, M. E.; Stavila, V.; Haney, P.; Kinney, R. A.; Szalai, V.; Gabaly, F. E.; Yoon, H. P.; Léonard, F.; Allendorf, M. D. *Science* **2014**, *343*, 66−69.
(12) Hendon, C. H.; Tiana, D.; Walsh, A. *Phys. Chem. Chem. Phys.* **2012**, *14*, 13120−13132.
(13) Kobayashi, Y.; Jacobs, B.; Allendorf, M. D.; Long, J. R. *Chem. Mater.* **2010**, *22*, 4120−4122.
(14) Allendorf, M. D.; Schwartzberg, A.; Stavila, V.; Talin, A. A. *Chem.—Eur. J.* **2011**, *17*, 11372−11388.
(15) Fuma, Y.; Ebihara, M.; Kutsumizu, S.; Kawamura, T. *J. Am. Chem. Soc.* **2004**, *126*, 12238−12239.

DOI: 10.1021/jacs.5b03263
J. Am. Chem. Soc. 2015, 137, 8169−8175

(16) Sheberla, D.; Sun, L.; Blood-Gorsythe, M. A.; Er, S.; Wade, C. R.; Brozek, C. K.; Aspuru-Guzik, A.; Dincă, M. *J. Am. Chem. Soc.* **2014**, *136*, 8859−8862.
(17) Narayan, T. C.; Miyakai, T.; Seki, S.; Dincă, M. *J. Am. Chem. Soc.* **2012**, *134*, 12932−12935.
(18) Uemura, T.; Uchida, N.; Asano, A.; Saeki, A.; Seki, S.; Tsujimoto, M.; Isoda, S.; Kitagawa, S. *J. Am. Chem. Soc.* **2012**, *134*, 8360−8363.
(19) Gándara, F.; Uribe-Romo, F. J.; Britt, D. K.; Furukawa, H.; Lei, L.; Cheng, R.; Duan, X.; O'Keeffe, M.; Yaghi, O. M. *Chem.—Eur. J.* **2012**, *18*, 10595−10601.
(20) Givaja, G.; Amo-Ochoa, P.; Gomez-Garcia, C. J.; Zamora, F. *Chem. Soc. Rev.* **2012**, *41*, 115−147.
(21) D'Alessandro, D. M.; Kanga, J. R. R.; Caddy, J. S. *Aust. J. Chem.* **2011**, *64*, 718−722.
(22) Yin, Z.; Wang, Q.-X.; Zeng, M.-H. *J. Am. Chem. Soc.* **2012**, *134*, 4857−4863.
(23) Dragasser, A.; Shekhah, O.; Zybaylo, O.; Shen, C.; Buck, M.; Wöll, C.; Schlettwein, D. *Chem. Commun.* **2012**, *48*, 663−665.
(24) Leonard, F.; Talin, A. A. *Nat. Nanotechnol.* **2011**, *6*, 773−783.
(25) Yoon, S. M.; Warren, S. C.; Grzybowski, B. A. *Angew. Chem., Int. Ed.* **2014**, *126*, 4526−4530.
(26) Gasteiger, H. A.; Kocha, S. S.; Sompalli, B.; Wagner, F. T. *Appl. Catal., B* **2005**, *56*, 9−35.
(27) Han, S.; Wei, Y.; Valente, C.; Forgan, R. S.; Gassensmith, J. J.; Smaldone, R. A.; Nakanishi, H.; Coskun, A.; Stoddart, J. F.; Grzybowski, B. A. *Angew. Chem., Int. Ed.* **2011**, *50*, 276−279.
(28) Wei, Y.; Han, S.; Walker, D. A.; Fuller, P. E.; Grzybowski, B. A. *Angew. Chem., Int. Ed.* **2012**, *51*, 7435−7439.
(29) Wilcoxon, J. P.; Martin, J. E.; Provencio, P. *J. Chem. Phys.* **2001**, *115*, 998−1008.
(30) Bakr, O. M.; Amendola, V.; Alkens, C. M.; Wenseleers, W.; Li, R.; Negro, L. D.; Schatz, G. C.; Stellaci, F. S. *Angew. Chem., Int. Ed.* **2009**, *121*, 6035−6040.
(31) Hsieh, C.-H.; Chou, L.-J.; Lin, G.-R.; Bando, Y.; Golberg, D. *Nano Lett.* **2008**, *8*, 3081−3085.
(32) Hu, M. S.; Chen, H.-L.; Shen, C. H.; Hong, L. S.; Huang, B. R.; Chen, K. H.; Chen, L. C. *Nat. Mater.* **2006**, *5*, 102−106.
(33) Huang, C.-H.; Lin, H. Y.; Lau, B. C.; Liu, C. Y.; Chui, H. C.; Tzeng, Y. *Opt. Express* **2010**, *18*, 27891−27899.
(34) Wessels, J. M.; Nothofer, H. G.; Ford, W. E.; von Wrochem, F.; Scholz, F.; Vossmeyer, T.; Schroedter, A.; Weller, H.; Yasuda, A. *J. Am. Chem. Soc.* **2004**, *126*, 3349−3356.
(35) Zabet-Khosousi, A.; Dhirani, A.-A. *Chem. Rev.* **2008**, *108*, 4072−4124.
(36) Warren, S. C.; Perkins, M. R.; Adams, A. M.; Kamperman, M.; Burns, A. A.; Arora, H.; Herz, E.; Suteewong, T.; Sai, H.; Li, Z.; Werner, J.; Song, J.; Werner-Zwanziger, U.; Zwanziger, J. W.; Grätzel, M.; DiSalvo, F. J.; Wiesner, U. *Nat. Mater.* **2012**, *11*, 460−467.
(37) Neugebauer, C. A.; Webb, M. B. *J. Appl. Phys.* **1962**, *33*, 74−82.
(38) Zallen, R. *The physics of amorphous solids*; Wiley-VCH Verlag GmbH & Co. KGaA: Weinheim, Germany, 1983.
(39) Zagorodniy, K.; Seifert, G.; Hermann, H. *Appl. Phys. Lett.* **2010**, *97*, 251905−251902.
(40) Chemical Rubber Company. *CRC handbook of chemistry and physics*, 79th ed., CRC Press: Boca Raton, FL, 1999.
(41) The dielectric constant of the MOF was calculated by determining the volume fraction of the MOF that is composed of open pore space (58.3%) and cyclodextrin (41.7%, percentages estimated in Materials Studio modeling environment). Dextrin has a dielectric constant of 2.3 (ref 31). We took an average of the dielectric constant of vacuum and dextrin, weighted by the relative volume fraction of each to get the estimated dielectric constant of 1.54. This is consistent with values that have been calculated elsewhere (ref 30).
(42) McCreery, R. L. *Chem. Mater.* **2004**, *15*, 4477−4496.
(43) Houk, R. J. T.; Jacobs, B. W.; Gabaly, F. E.; Chang, N. N.; Talin, A. A.; Graham, D. D.; House, S. D.; Robertson, I. M.; Allendorf, M. D. *Nano Lett.* **2009**, *9*, 3413−3418.
(44) Juan-Alcaniz, J.; Gascon, J.; Kapteijn, F. *J. Mater. Chem.* **2012**, *22*, 10102−10118.
(45) Warren, S. C.; Voïtchovsky, K.; Dotan, H.; Leroy, C. M.; Cornuz, M.; Stellacci, F.; Hébert, C.; Rothschild, A.; Grätzel, M. *Nat. Mater.* **2013**, *12*, 842−849.
(46) The Rb-CD-MOF is a cubic crystal with channels being identical in all three orthogonal directions; in other words, there is no anisotropy in this system that might affect conductivity in different directions. While the MIL-53(Al) is anisotropic, our experiments were performed on polycrystalline films, and thus any anisotropic effects could not be measured. In general, the tunneling barriers and average tunneling distances will certainly be anisotropic in systems with 1D or 2D channels, but given that tunneling can easily occur at distances up to 3 nm (see Choi, S. H.; Kim, B. S.; Frisbie, C. D. *Science* **2008**, *320*, 1482−1486), we do not expect that conductivity will ever be fully blocked in directions that are perpendicular to channels.
(47) Huynh, M. H. V.; Meyer, T. J. *Chem. Rev.* **2007**, *107*, 5004−5064.

DOI: 10.1021/jacs.5b03263
J. Am. Chem. Soc. 2015, 137, 8169−8175